

NOVEL NEUTRON-DRIVEN CYCLIC REACTION IN THE FORMATION OF POLONIUM-210

Solomon Lim¹ and Pong Boon Kin²

¹NUS High School of Mathematics and Science, 20 Clementi Ave 1, Singapore 129957

²DSO National Laboratories, 12 Science Park Drive, Singapore 118225

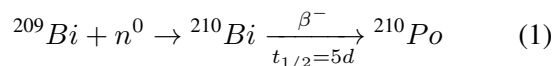
Abstract

In this study, a previously undescribed cyclic nuclear reaction based on neutron-driven interactions was investigated. The cyclic reaction could potentially enhance the production efficiency of polonium-210, which is a radioisotope of industrial significance. Initiated by an external neutron source, the cyclic reaction occurs in four steps. Absorption of neutrons by bismuth-209 leads to the formation of short-lived bismuth-210 which beta-decay to form polonium-210. The alpha particles emitted by polonium-210 would then react with beryllium-9 to form an “internal” source of neutrons, driving a chain reaction in a cyclic manner. Retrofunctional analysis of the cyclic reaction identified the elemental composition of bismuth beryllium acetate (BBA) to be optimal for (i) internal neutron production by beryllium, (ii) neutron thermalization by acetate, and (iii) neutron absorption by bismuth. The prepared BBA salt was characterized with ICP-MS spectrometry and SEM microscopy. To initiate the cyclic reaction, the BBA salt was irradiated with thermalized neutron fluxes from a californium-252 neutron source. Gamma spectroscopy was used to demonstrate neutron emission from the irradiated material, confirming that the cyclic reaction has occurred. Evidence of the cyclic reaction was also obtained through the observed autocatalytic reaction kinetics.

Introduction

Background and Purpose

Since the discovery of the neutron by James Chadwick in 1932 [1], neutron-mediated nuclear reactions have been utilised in a myriad of contemporary innovations, such as (n,α) reactions in boron neutron capture therapy [2] and radiative neutron capture in neutron activation analysis [3]. In particular, the industrially significant radioisotope polonium-210 (²¹⁰Po), which has numerous uses as a radiotherapeutic agent [4] and in satellite power generators [5], is formed as a neutron activation product from natural bismuth (²⁰⁹Bi) as shown in (1):



Interestingly, ²¹⁰Po (a strong alpha emitter) is also utilised in neutron sources via (α,n) reaction with low-Z materials such as beryllium [6]. This leads to the project’s conjecture of a previously undescribed cyclic nuclear reaction in which *neutrons produced from decaying ²¹⁰Po can be harnessed to produce more*

²¹⁰Po, whereby the alpha particles emitted by ²¹⁰Po are used to produce neutrons through (α,n) reaction with ⁹Be to activate even more ²⁰⁹Bi atoms. The cyclic reaction is depicted in Figure 1.

However, the aforementioned cyclic reaction would require a suitable environment to minimise neutron losses and sustain the cyclic propagation. Based on existing studies by Michaud *et al.* on enhanced neutron production in intermetallic beryllides due to the atomic homogenisation within ionic lattices [7], as well as research by Fiorito *et al.* on the energy-dependence of the bismuth neutron capture cross section [8], retrofunctional analysis was utilised in this study to design and synthesise a salt with the required properties to sustain the cyclic reaction.

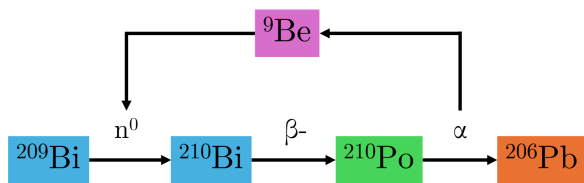


Fig. 1: Diagram of cyclic reaction mechanism

Hence, the validation of the cyclic reaction is accomplished by exposing the salt to thermal neutrons to initiate the reaction, and two complementary methods are used to confirm the successful occurrence of the reaction - gamma spectroscopic analysis to demonstrate neutron emission from the salt, and temporal analysis to demonstrate cyclic behaviour. This also represents a novel method of ^{210}Po formation that can potentially be translated into industrial processes for rapid and large-scale production of radiotherapeutic agents like ^{210}Po .

Hypothesis

In this study, we aim to validate a novel cyclic nuclear reaction comprising of four steps:

1. Neutron capture by ^{209}Bi , forming ^{210}Bi
2. Beta decay of ^{210}Bi to ^{210}Po
3. Alpha particle emission from ^{210}Po
4. Neutron emission from ^9Be from (α, n) reaction

Methodology

The cyclic reaction setup contained three components - a salt, where the reaction occurs, a neutron source to irradiate the salt, and a moderator assembly to optimise the thermal neutron flux.

Salt design and synthesis

For the cyclic reaction to occur, the salt was designed to meet three important criteria:

1. Large (α, n) cross section for neutron generation;
2. High hydrogen density to thermalise the neutrons to achieve efficient capture of the neutrons by ^{209}Bi to produce ^{210}Bi [9];
3. High ^{209}Bi density to maximise neutron capture.

For criterion 1, beryllium-9 was chosen as a key component of the salt due to its high (α, n) cross section compared to other elements [10] as shown in Fig. 2. Furthermore, beryllium possesses a relatively large ($n, 2n$) cross section used for neutron multiplication in fusion reactors, which would compensate for neutron leakage [11].

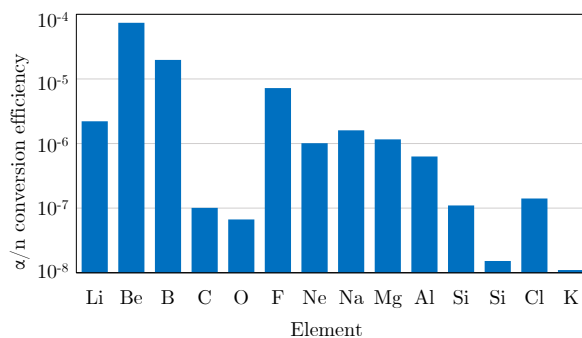


Fig. 2: (α, n) yields for selected elements

For criteria 2 and 3, acetate (CH_3COO^-) was chosen as the counterion for its high hydrogen content, which increases neutron moderation [12]. In addition, this also increases the atomic density of ^{209}Bi as observed in basic acetate salts, due to the acetate ions acting as bidentate bridging ligands [13] and increasing the proximity of metal centers [14] as shown in Fig. 3. Hence, the novel compound bismuth beryllium acetate (BBA, $\text{BiBe}_2\text{O}(\text{CH}_3\text{COO})_5$) was chosen.

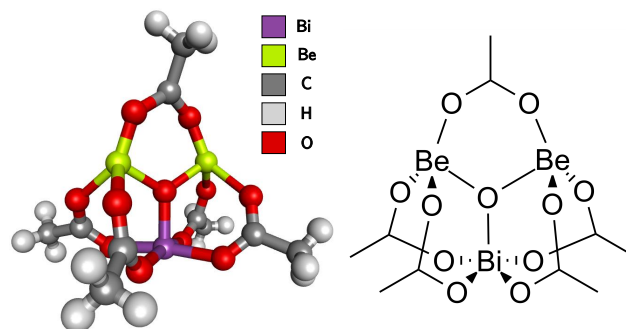


Fig. 3: Predicted molecular structure of BBA

The detailed procedure for the synthesis of BBA can be found in Appendix A - briefly, bismuth trioxide and beryllium sulfate were dissolved in a solution of peroxyacetic acid, followed by coprecipitation with concentrated sodium hydroxide and particulate microinfiltration with beryllium sulfate to yield the amorphous salt.

The elemental composition of the salt was analysed with inductively-coupled plasma mass spectrometry (ICP-MS) on the Agilent 7850 ICP mass spectrometer, utilising helium collision cells [15] and half mass correction [16] to reduce polyatomic and doubly-charged ionic interference. Salt morphology was characterised with scanning electron microscopy (SEM) on the Phenom Desktop SEM with full backscattered electron detection [17].

Neutron source characterisation

A $5\mu\text{Ci}$ ^{252}Cf neutron source was used to irradiate the BBA salt sample, providing a neutron output of $2.05 \times 10^4 \text{ n s}^{-1}$ [18]. The energy spectrum of the neutron source was measured using an ARKTIS S670e $^4\text{He}/^6\text{Li}$ neutron detector. Energy-channel calibration is achieved using maxima-corrected retrotransposition [19] and cross-validated with a Maxwellian spectrum-folding method derived from the detector response matrix [20] as shown in (2):

$$N(x) = \int R(x, E_n) \Phi(E_n) dE_n \quad (2)$$

where $N(x)$ is the folded intensity, $R(x, E_n)$ is the detector response matrix, and $\Phi(E_n)$ is the corrected Maxwellian neutron spectrum.

Neutron irradiation assembly

To initiate the reaction, a 40.0g sample of BBA was irradiated with thermalised neutrons from the ^{252}Cf neutron source in a polyethylene flux-optimised scattering assembly (FOSA) [21] for 16h as shown in Fig. 4. Monte Carlo computational modelling of the FOSA setup with OpenMC [22] was also used to demonstrate the increased thermal flux compared to a conventional linear irradiation setup.

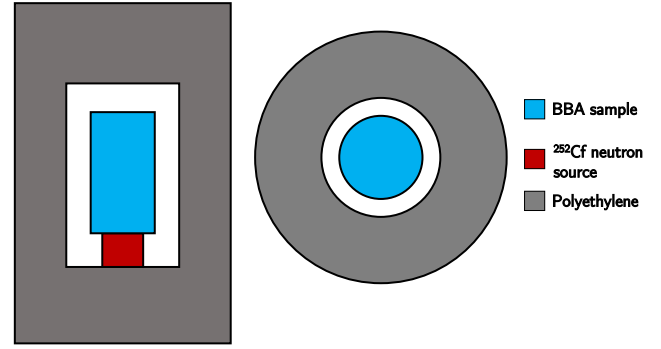


Fig. 4: Diagram of FOSA assembly (left: front view, right: top view)

Cyclic reaction validation

Two methods were used to conclusively prove the occurrence of the cyclic reaction - neutron detection and temporal analysis.

Firstly, a key indicator of the cyclic reaction is the emission of neutrons from (α, n) reactions within the BBA salt matrix. This results from the mechanism of the cyclic reaction, i.e. neutron emission can only occur if (α, n) reactions have occurred, which in turn can only occur if ^{210}Po has been formed, as ^{210}Po is the only source of α particles in the reaction mixture and there are no other significant neutron-producing reactions occurring. Hence, it is readily apparent that the emission of neutrons is intrinsically correlated to the propagation of the cyclic reaction.

Neutron emission was analysed using an ORTEC high-resolution HPGe gamma spectrometer via detection of the 2.2 MeV gamma photopeak resulting from the radiative capture of thermal neutrons by ^1H atoms [23], which has been utilised as a well-described and reliable method of neutron detection in previous studies due to its significant cross section of 0.33b [24, 25, 26, 27]. Hence, the presence of the 2.2 MeV photopeak demonstrates the successful occurrence of the reaction.

Secondly, to prove that the reaction obeys cyclic kinetics, the post-irradiation evolution of ^{210}Po accumulation is derived from (α, n) backconversion

to obtain the supposed nimety, and contrasted with conventional first-order decay kinetics to demonstrate the resultant occurrence of secondary ^{210}Po generation from the cyclic reaction. This was achieved by considering the simplified kinetic equation for conventional ^{210}Po production [28]:

$$N_{Po}(t) = \frac{N_{Bi}\sigma_c\Phi_{Cf}}{\lambda_{Po} + \lambda_{Bi}}(1 - e^{-(\lambda_{Po} + \lambda_{Bi})T})(e^{-\lambda_{Po}(t-T)}) \quad (3)$$

where $N_{Po}(t)$ is the number of ^{210}Po atoms at time t after irradiation, N_{Bi} is the initial number of bismuth atoms, σ_c is the neutron capture cross section, Φ_{Cf} is the neutron flux, λ_{Po} and λ_{Bi} are the decay constants of ^{210}Po and ^{210}Bi respectively, and T is the irradiation time. However, the cyclic reaction would result in a modified kinetic:

$$N_{Po}(t) = \frac{N_{Bi}\sigma_c\Phi_T}{\lambda_{Po} + \lambda_{Bi}}(1 - e^{-(\lambda_{Po} + \lambda_{Bi})T})(e^{-\lambda_{Po}(t-T)}) \quad (4)$$

$$\Phi_T = \Phi_{Cf} + \frac{\eta_{Be}N_{Po}(t)\phi_{Be}}{N_{Be}} \quad (5)$$

where Φ_T is the total neutron flux, η_{Be} is the (α, n) conversion factor, ϕ_{Be} is the dispersion coefficient, and N_{Be} is the number of beryllium atoms.

Hence, by solving Eq. (4) iteratively, the reaction kinetics of the experimental sample can be elucidated and shown to obey cyclic kinetics, thus demonstrating that the cyclic reaction has occurred.

Results and Discussion

Salt characterisation

The ICP-MS calibration curve of BBA is shown in Fig. 5. After calibration with beryllium and bismuth standard solutions, the atomic ratio of beryllium to bismuth in the salt was found to be 2.050, in good agreement with the predicted ratio of 2.000, with the formula $\text{BiBe}_2\text{O}(\text{CH}_3\text{COO})_5$ and a hydrogen content of 2.79%. This indicates excellent moderation capability, as most bismuth compounds have a much lower hydrogen content, including bismuth hydride (1.42%).

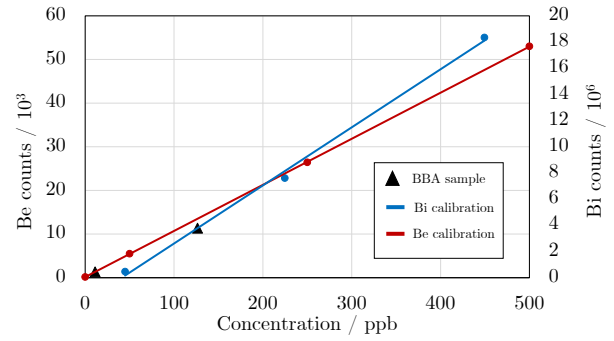


Fig. 5: ICP-MS calibration curves for Bi and Be

SEM characterisation of BBA shown in Fig. 6 also revealed a highly porous, amorphous morphology containing reticulated acicular aggregates 1 - 5 μm in length. This suggests a high affinity for substrate absorption [29], which can be used to adjust the bismuth or beryllium content of the reaction mixture as required via microinfiltration.

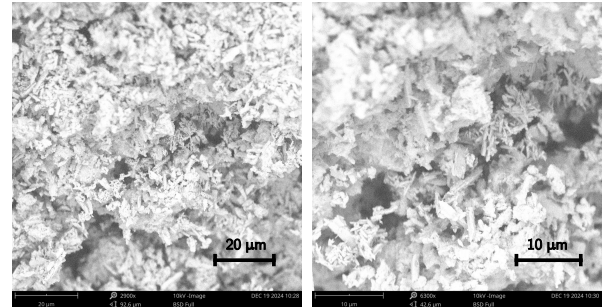


Fig. 6: SEM images of the BBA salt sample

Hence, basic elemental and morphological methods of characterisation have been carried out on the previously-undescribed BBA salt, demonstrating its suitability for the cyclic reaction.

Neutron irradiation analysis

As observed from Fig. 7, the experimental neutron spectrum of the ^{252}Cf neutron source demonstrated good agreement with literature standards [30, 31], with a peak energy of 2.1 MeV. This also confirmed the utility of the FOSA assembly in ensuring maximal moderation of the fast neutrons emitted.

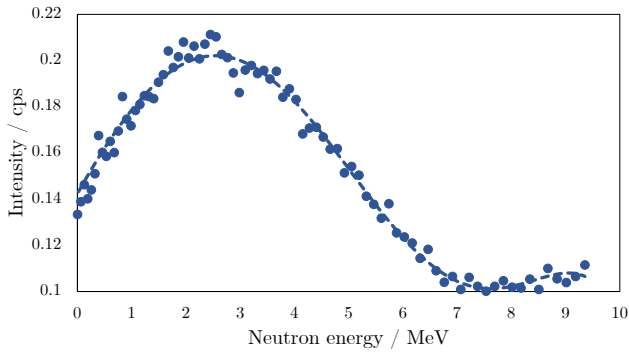


Fig. 7: Neutron spectrum of the ^{252}Cf source

The result of the Monte Carlo OpenMC models are presented in Fig. 8, which compares the fast and thermal neutron flux between a conventional linear irradiation assembly and the FOSA assembly. The FOSA assembly was shown to increase fast neutron flux by a factor of 4.6, while thermal neutron flux was increased by a factor of 12.9 with respect to the irradiation position.

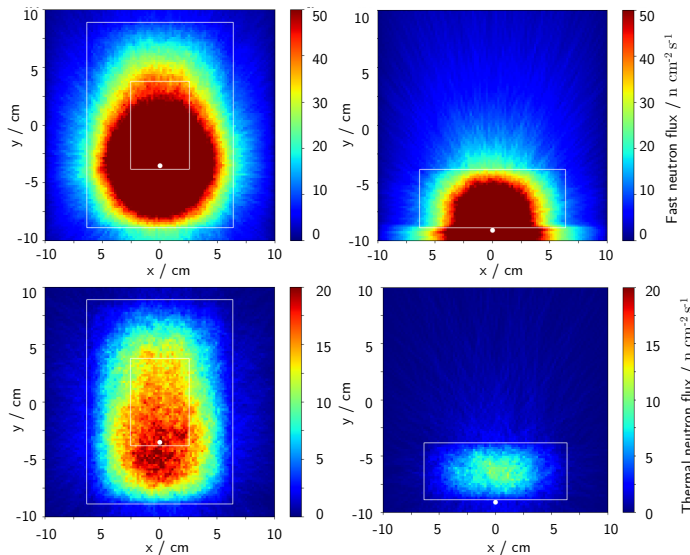


Fig. 8: Fast(top) and thermal(bottom) flux in FOSA(left) vs conventional assembly(right)

The efficacy of the FOSA system can be attributed to the isotropic angular distribution of neutron scattering [32], resulting in Markovian transport dynamics within the polyethylene walls [33], i.e. some neutrons are backscattered towards the source. Hence, the container walls serve to thermalise and "reflect" neutrons towards

the irradiation cavity, in addition to ensuring greater irradiation homogeneity, as the backscattered neutrons would emerge from all points in the irradiation cavity. Hence, a thermal neutron flux of $20 \text{ n cm}^{-2} \text{ s}^{-1}$ was achieved using the FOSA assembly.

Cyclic reaction validation

Firstly, neutron detection is used to demonstrate the occurrence of the cyclic reaction. As shown in Fig. 9, the 2.2 MeV photopeak was detected with a peak area of 695 counts (background-corrected), which indicates a significant rate of neutron emission from the irradiated BBA and showing that the cyclic reaction had occurred. Furthermore, as the 2.2 MeV photopeak is associated with thermal neutron capture from ^1H atoms, this also demonstrates the neutron moderation properties of the BBA salt as it is able to successfully thermalise the fast neutrons emitted by ^{210}Po atoms, increasing the thermal neutron population for subsequent cycles of neutron capture.

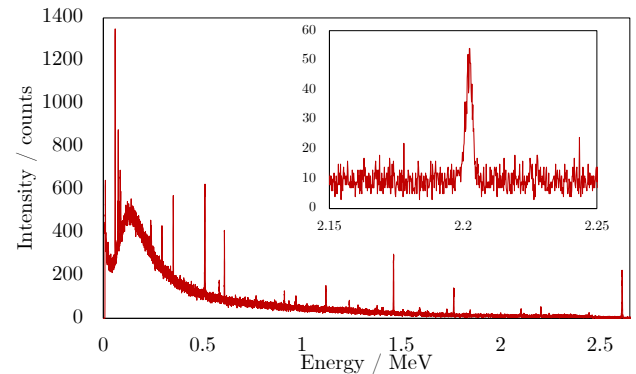


Fig. 9: Gamma-spectrum of irradiated BBA

The chemical composition of the BBA salt also highlights the utility of neutron detection compared to directly measuring α emissions from ^{210}Po , or even β^- emissions from ^{210}Bi , as the high bismuth atomic density confers a relatively high stopping power and a simulated mean ionisation energy of 180.6 eV to the bulk salt material [34], which results in a low α escape probability and the absorption of a majority of β^- particles with the release of non-characteristic bremsstrahlung radiation [35].

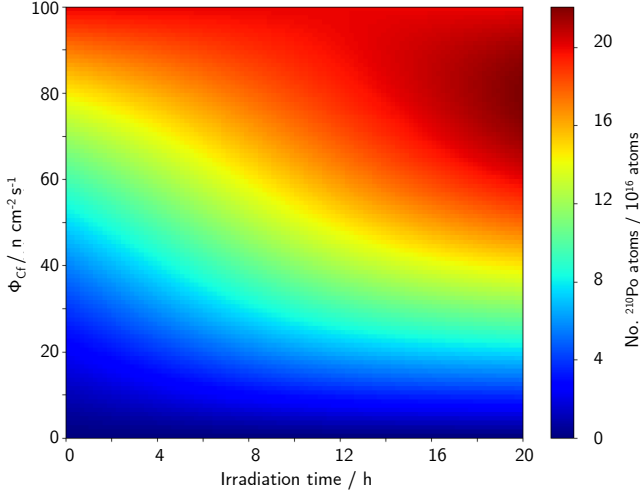


Fig. 10: Effect of irradiation flux on ^{210}Po accumulation

In addition, the reaction progress was also able to be determined from the Gaussian parameters of the neutron photopeak. As the peak area of the photopeak can be used to obtain the neutron emission rate of the BBA sample using Eq. (6), this can be correlated with an systematic equation Eq. (7) relating neutron emission to the n th cycle of the cyclic reaction:

$$A = \frac{hw}{2\mu_E\sigma_H\rho rt} \sqrt{\frac{\pi}{\ln 2}} \quad (6)$$

$$A_n = \frac{\mu}{1 + \frac{\mu-b}{b} e^{-k\psi n}} \quad (7)$$

where h is the peak height, w is the peak full width at half maximum (FWHM), μ_E is the detector efficiency at 2.2 MeV, t is the detector live time, σ_H is the ^1H neutron capture cross section, ρ is the atomic density of BBA, r is the radius of the irradiation container, k is the (α, n) conversion efficiency, μ is the equilibrium limit correlating neutron propagation and leakage, b is the minimum limit, and ψ is the predicted growth rate.

It was calculated that the irradiated BBA sample has a neutron emission rate of 0.418 n s^{-1} , which corresponds to $n \approx 2$, i.e. the reaction has completed more than one cycle. We are also able to observe from Eq. (7) that the neutron production rate will obey sigmoidal kinetics due to an initial rapid increase in neutron emissions when

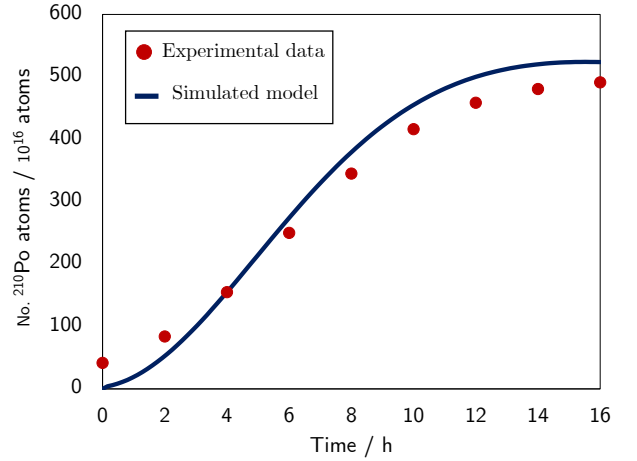


Fig. 11: Comparison of experimental and predicted kinetics

neutron capture is occurring rapidly in the BBA salt, after which the neutron emission rate will slow down and plateau as each cycle generates less ^{210}Po than the previous cycle. Hence, this further confirms the cyclic nature of the reaction by demonstrating that the reaction is able to sustain at least one complete iteration of the mechanism.

Secondly, temporal analysis is also used to characterise the ^{210}Po accumulation kinetics of the cyclic reaction in order to demonstrate pseudo-autocatalytic dynamics. As shown in Fig. 10, the amount of ^{210}Po in the BBA salt sample increases sigmoidally with respect to time, while it asymptotically increases with respect to the initial irradiation flux.

The sigmoidal kinetics with respect to time are attributed to an initial rapid increase due to a high rate of ^{209}Bi neutron capture from the relatively strong irradiation flux, before the growth rate slows down as each cycle generates less ^{210}Po than the previous cycle, similar to the neutron emission rate. The effect of irradiation flux on the ^{210}Po growth rate is particularly evident at low fluxes, as the initial rapid rate of neutron capture and ^{210}Po formation is directly correlated to the irradiation flux, which acts as a "trigger" for

the reaction. However, at high fluxes, the effect of irradiation flux becomes less pronounced due to the equilibrium limit of ^{209}Bi neutron capture.

Figure 11 also shows the experimentally determined ^{210}Po accumulation curve based on cubic spline interpolation of the data derived from the (α, n) conversion efficiency. Coincidentally, this data also demonstrates good agreement with the OpenMC model of the irradiation assembly, which yields a thermal neutron flux of approximately $20 \text{ n cm}^{-2} \text{ s}^{-1}$.

Ultimately, this also serves to confirm that the cyclic reaction has taken place in the irradiated BBA salt sample due to the characteristic sigmoidal nature of the reaction. Furthermore, we are also able to compare the amount of ^{210}Po formed based on cyclic and conventional irradiation kinetics from Eq. (3) and (4) respectively.

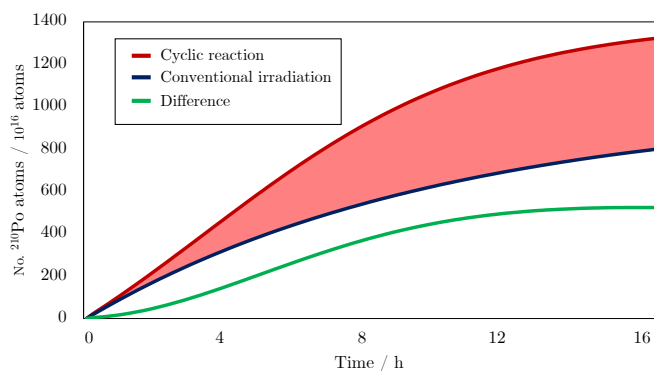


Fig. 12: Derivation of irradiation accumulation curve

As shown in Fig. 12, the experimentally obtained value for the amount of ^{210}Po formed is significantly higher than the predicted amount formed under conventional irradiation [36] while demonstrating good agreement with cyclic kinetics, thus further evidencing the successful occurrence of the cyclic chain reaction by demonstrating that secondary cycles of ^{210}Po formation must have taken place in order to rationalise the surplus of ^{210}Po obtained in the BBA salt sample. Fig. 12 also shows that the total amount of ^{210}Po formed in the BBA

salt under irradiation is equal to the aggregate sum of the ^{210}Po formed from irradiation and the cyclic reaction, which is consistent with theoretical predictions.

Hence, it has been conclusively shown using complementary methods of analysis that the novel cyclic nuclear reaction has occurred in the BBA salt sample by showing that (1) neutrons are emitted from the reaction, (2) the reaction has completed at least one full cycle, (3) the reaction obeys cyclic kinetics, and (4) more ^{210}Po is formed than predicted under conventional irradiation conditions.

Conclusion

In conclusion, we have experimentally demonstrated the existence of a novel cyclic nuclear reaction resulting in the formation of the industrially significant radioisotope ^{210}Po . The cyclic reaction was successfully initiated in a novel salt, bismuth beryllium acetate (BBA) via thermal neutron irradiation using a ^{252}Cf neutron source housed in a flux-optimised scattering assembly. Evidence of the novel cyclic nature of the reaction was obtained by gamma-neutron detection and temporal reaction kinetic analysis.

Limitations

The direct detection of ^{210}Po formation via alpha spectroscopy or liquid scintillation counting (LSC) is limited by the thermal neutron flux from the irradiation assembly, which is relatively low ($10^4 \text{ n cm}^{-2} \text{ s}^{-1}$) compared to conventional irradiation sources ($10^7 - 10^{11} \text{ n cm}^{-2} \text{ s}^{-1}$). Hence, more conclusive evidence for the occurrence of the cyclic reaction can be obtained with a stronger neutron source.

Furthermore, due to radiation safety regulations, real-time gamma analysis of the reaction mixture under neutron irradiation is unable to be obtained, instead being limited to post-irradiation analysis and indirect gamma-neutron detection. Hence, mobile remote gamma spectrometers with discriminatory capabilities

can be utilised to monitor the neutron emission rate of the BBA salt sample during the irradiation period, allowing for the complete kinetics to be fully characterised.

Future Work

In future studies, this cyclic reaction can be scaled up in order to produce ^{210}Po in industrially useful quantities. Not only would this provide a cheap, rapid method of producing ^{210}Po , the inherently autocatalytic nature of the reaction would also reduce dependence on commercial nuclear reactors as a strong initial irradiation flux is no longer required. A chemical method of separating and purifying the ^{210}Po from the irradiated BBA salt can also be further developed in order to further utilise the ^{210}Po produced in the cyclic reaction. This would also aid the production of ^{210}Po compounds, e.g. ligand-tagged radiotherapeutic agents from the bismuth feedstock.

This cyclic mechanism can also be applied to the production of other industrially-significant radioisotopes such as cobalt-60, using photoneutron production instead of (α, n) reactions. This would allow for greater robustness and versatility in utilising the self-propagation properties of the reaction to improve a wider range of existing radioisotope production methods.

Acknowledgements

We would like to thank our mentor Dr Pong Boon Kin for his valuable guidance throughout the project. In addition, we also thank Mr Mak Jia Feng for his assistance with neutron calibration measurements, gamma spectroscopy and SEM microscopy, Ms Evelyn Low for her help with the chemical synthesis of the BBA salt, Dr Doris Ho for her assistance with ICP-MS spectrometry, and Ms Lee Hui Min for her help with liquid scintillation counting.

References

1. James Chadwick. The existence of a neutron. *Proceedings of the Royal Society of London Series a Containing Papers of a Mathematical and Physical Character*, 136(830):692–708, June 1932.
2. Huifang He, Jiyuan Li, Ping Jiang, Suqing Tian, Hao Wang, Ruitai Fan, Junqi Liu, Yuyan Yang, Zhibo Liu, and Junjie Wang. The basis and advances in clinical application of boron neutron capture therapy. *Radiation Oncology*, 16(1), November 2021.
3. Debashree Debasish Das, Nikita Sharma, and Pooja A Chawla. Neutron activation analysis: an excellent nondestructive analytical technique for trace metal analysis. *Critical Reviews in Analytical Chemistry*, page 1–17, February 2023.
4. Michael K. Schultz, Mark P. Borgman, Tomika Coleman, Sergei Bakhlanov, Nikolai Marchenkov, and Bruce R. Line. An assessment of radionuclidic impurities of ^{210}Po produced via neutron irradiation of ^{209}Bi for use in targeted alpha-particle radiotherapy. *Applied Radiation and Isotopes*, 65(7):784–792, March 2007.
5. R.C. O'Brien, R.M. Ambrosi, N.P. Bannister, S.D. Howe, and H.V. Atkinson. Safe radioisotope thermoelectric generators and heat sources for space applications. *Journal of Nuclear Materials*, 377(3):506–521, April 2008.
6. J L Richmond. Neutron, alpha, and special sources from polonium. Technical report, Mound Laboratory (MOUND), Miamisburg, OH (United States), 06 1954.
7. G. G. Michaud and R. R. Boucher. Neutron sources from the beryllium reduction of plutonium dioxide. *Canadian Journal of Physics*, 38(4):555–564, April 1960.
8. Luca Fiorito, Alexey Stankovskiy, Augusto Hernandez-Solis, Gert Van Den Eynde, and Gasper Žerovnik. Nuclear data uncertainty analysis for the ^{210}Po production in myrrha. *EPJ Nuclear Sciences Technologies*, 4:48, January 2018.

9. K. Saito, M. Igashira, J. Kawakami, T. Ohsaki, T. Obara, and Hiroshi Sekimoto. Measurement of kev-neutron capture cross section of bi-209. 06 2003.
10. R. Heaton, H. Lee, P. Skensved, and B.C. Robertson. Neutron production from thick-target (γ, n) reactions. *Nuclear Instruments and Methods in Physics Research Section a Accelerators Spectrometers Detectors and Associated Equipment*, 276(3):529–538, April 1989.
11. R. Gaisin, R. Rolli, V. Chakin, and P. Vladimirov. Beryllides as advanced materials for neutron multiplication, 2023.
12. M.M. Hosamani, A. Vinayak, G.B. Hiremath, Prashant N. Patil, and N.M. Badiger. Determination of neutron moderation parameters through neutron captured gamma ray emission – a novel method. *Annals of Nuclear Energy*, 171:109045, March 2022.
13. B. N. Figgis and G. B. Robertson. Crystal-molecular structure and magnetic properties of $\text{Cr}_3(\text{CH}_3\text{COO})_6\text{OCl}_5\text{H}_2\text{O}$. *Nature*, 205(4972):694–695, February 1965.
14. William Henry Bragg and Gilbert Thomas Morgan. Crystal structure and chemical constitution of basic beryllium acetate and propionate. *Proceedings of the Royal Society of London Series a Containing Papers of a Mathematical and Physical Character*, 104(727):437–451, November 1923.
15. Mónica Iglesias, Nicole Gilon, Emmanuelle Poussel, and Jean-Michel Mermet. Evaluation of an icp-collision/reaction cell-ms system for the sensitive determination of spectrally interfered and non-interfered elements using the same gas conditions. *Journal of Analytical Atomic Spectrometry*, 17:1240, 09 2002.
16. Skyler W. Smith, Roy W. Martin, Nicole Hanks, Patricia A. Creed, Kasey Kovalcik, Robert A. Wilson, Kevin Kubachka, Judith A. Brisbin, Julio a. Landero Figueroa, and John T. Creed. An evaluation of m2+ interference correction approaches associated with as and se in icp-ms using a multi-day dataset along with icp-ms/ms/hr-icp-ms based analysis and hierarchical modeling as a means of assessing bias in fortified drinking waters and single component matrices. *Journal of Analytical Atomic Spectrometry*, 37(4):898–909, January 2022.
17. Pavel Kejzlar, Martin Švec, and Eva Macajová. The usage of backscattered electrons in scanning electron microscopy. *Manufacturing Technology*, 14:333–336, 10 2014.
18. R.C Martin, J.B Knauer, and P.A Balo. Production, distribution and applications of californium-252 neutron sources. *Applied Radiation and Isotopes*, 53(4–5):785–792, November 2000.
19. Cathleen Barker, Ting Zhu, Lucas Rolison, Scott Kiff, Kelly Jordan, and Andreas Enqvist. Pulse shape analysis and discrimination for silicon-photomultipliers in helium-4 gas scintillation neutron detector. *EPJ Web of Conferences*, 170:07002, January 2018.
20. Paolo Tancioni, Rico Chandra, Marco Panniello, Ulisse Gendotti, and Arktis Radiation Detectors Ltd. *Fast neutron dose rate monitoring using off the shelf Helium-4 scintillation detectors*, volume No. 62. June 2021.
21. Elsayed Elmaghraby, Eman Salem, Zeinab Yousef, and Nermin El-Anwar. Role of isomeric state formation on the measurement of thermal neutron cross section and resonance integral. *Physica Scripta*, 94, 01 2019.
22. Paul K. Romano, Nicholas E. Horelik, Bryan R. Herman, Adam G. Nelson, Benoit Forget, and Kord Smith. Openmc: A state-of-the-art monte carlo code for research and development. *Annals of Nuclear Energy*, 82:90–97, August 2014.
23. Víctor Hernandez-Davila, R. Villasana, Enma Acuña, John Ramirez Gonzalez, E.D. Felix, and Hector Vega-Carrillo. Monte carlo study to measure the neutron flux using the prompt gamma-rays in hydrogen. *Revista Mexicana de Física*, 53, 02 2007.
24. H. T. Wang, R. Ramaty, Goddard Space Flight Center, and University of Maryland. *NEUTRON PROPAGATION AND 2.2 MEV GAMMA-RAY LINE*

PRODUCTION IN THE SOLAR ATMOSPHERE.
January 1974.

25. H.R. Vega-Carrillo, E. Manzanares-Acuña, V.M. Hernández-Davila, E.D. Rodarte Felix, J. Ramirez-Gonzalez, R. Hernández Villasana, and Universidad Autonoma de Zacatecas Cuerpo Academico de Radiobiologia, Unidad Academica de Estudios Nucleares. *Monte Carlo study to measure the neutron flux using the prompt gamma-rays in hydrogen*, volume S53. August 2006.
26. Alvie Asuncion-Astronomo, Charlotte V. Balderas, Jeffrey D. Tare, and Cheri Anne M. Dingle. Neutron source strength verification via reaction rate measurement and monte carlo simulation. *Radiation Measurements*, 170:107050, December 2023.
27. Zachary Harvey. Neutron flux and energy characterization of a plutonium-beryllium isotopic neutron source by monte carlo simulation with verification by neutron activation analysis. 01 2010.
28. Potential for production of proliferation sensitive materials in research reactors. *Australian Safeguards Support Program*, March 2008.
29. Z. Sidorski, S. Zuber, and J. Polański. Adsorption of beryllium on (211) oriented tungsten single crystal: Work function changes and energy losses of scattered electrons. *Surface Science*, 80:626–636, February 1979.
30. L. Green, J. A. Mitchell, and N. M. Steen. The californium-252 fission neutron spectrum from 0.5 to 13 mev. *Nuclear Science and Engineering*, 50(3):257–272, March 1973.
31. W Mannhart. Status of cf-252 neutron spectrum as a standard. *Reactor Dosimetry: Methods, Applications, and Standardization*, page 340–347, January 1989.
32. R.O Lane, A.S Langsdorf, J.E Monahan, and A.J Elwyn. The angular distributions of neutrons scattered from various nuclei. *Annals of Physics*, 12(2):135–171, February 1961.
33. D.C. Sahni. An application of reactor noise techniques to neutron transport problems in a random medium. *Annals of Nuclear Energy*, 16(8):397–408, January 1989.
34. Martin Berger, J Coursey, and M Zucker. Estar, pstar, and astar: Computer programs for calculating stopping-power and range tables for electrons, protons, and helium ions (version 1.21), 1999-01-01 1999.
35. Shima K, Mihara T, Umetani K, and Mikumo T. [contribution of 210bi beta-ray induced bremsstrahlung to the emission of pb-kx-rays observed in the lead shielded gamma-ray background spectrum (author’s transl)]. *PubMed*, 29(8):363–7, August 1980.
36. B. Cameron Reed. Rousing the dragon: Polonium production for neutron generators in the manhattan project. *American Journal of Physics*, 87(5):377–383, April 2019.

Appendix A: Salt synthesis and characterisation

Synthesis of bismuth beryllium acetate (BBA)

All steps of the synthesis were carried out in a glovebox due to beryllium toxicity.

Beryllium metal (0.50g, 55.6mmol) was dissolved in 98% sulfuric acid (10mL), and the resultant solution of beryllium sulfate is slowly added to peroxyacetic acid (30mL) prepared from glacial AcOH (20mL) and 30% H₂O₂ (10mL). Bismuth trioxide (12.80g, 27.5mmol) was then dissolved in the reaction mixture under constant stirring, resulting in the formation of a yellow suspension. Significant effervescence was observed after 2h, accompanied by the formation of a white suspension. 50% sodium hydroxide is then added to the reaction mixture to obtain a brown precipitate, which was filtered under vacuum and washed with water thrice. The resultant powder is then dried under IR irradiation to obtain the crude BBA salt, which is further recombined via heterogenous infiltration with a saturated solution of beryllium sulfate in 98% sulfuric acid to obtain BBA as a dark yellow solid in good yield (15.09g, 84.1%).



Fig. 13: *Bismuth trioxide suspension before precipitation*



Fig. 14: *Bismuth trioxide suspension after precipitation with concentrated NaOH*

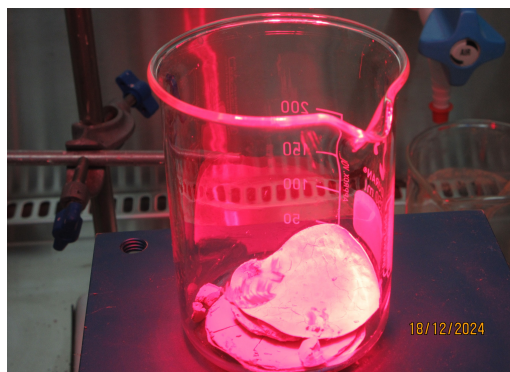


Fig. 15: *BBA drying under IR irradiation*

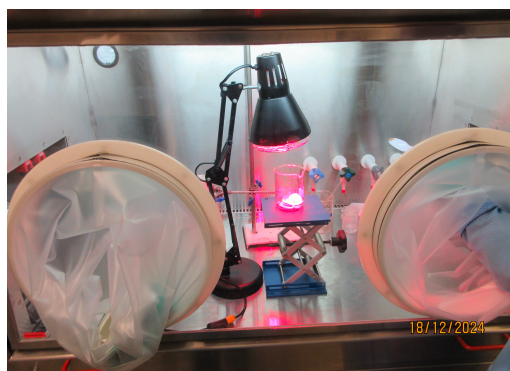


Fig. 16: *IR irradiation setup*

ICP-MS sample preparation

Two sets of ICP-MS samples were prepared for analysis - a calibration standard and the BBA sample itself. Three calibration standards were used to obtain a linear calibration curve, with concentrations of 50ppb, 250ppb, and 500ppb.

To prepare the calibration standards, 1000 ppm bismuth trioxide solution (50mL) was first prepared by dissolving bismuth trioxide powder (0.05g) in 63% nitric acid (1.0mL) before dilution with water (49.0mL). 1000 ppm beryllium solution (50mL) was also prepared by dissolving beryllium metal (0.05g) in 98% sulfuric acid (1.0mL) before dilution with water (49.0mL). The two solutions are then combined in equal quantities (1.0mL each) and serially diluted to obtain calibration solutions of the appropriate concentration.

To prepare the BBA analyte solution, BBA powder (0.05g) was dissolved in a mixture of sulfuric acid and nitric acid (0.5mL of 98% H_2SO_4 with 0.5mL of 63% HNO_3) before being serially diluted to obtain an analyte solution with a predicted concentration of 400ppb.

Structural analysis of BBA

The open-source crystal structure prediction software CrysPY is used to determine stable structures of the BBA salt based on the molecular formula obtained from ICP-MS analysis and similar structures, e.g. ferric acetate and basic beryllium acetate. Both the Random Search and Evolutionary Algorithm functions were utilised and compared to obtain complementary results, which provided vital structural information about the acetate ligand coordination in BBA and metal center proximity, which affects the macroscopic efficiency of (α, n) reactions by affecting the absorption of alpha particles by non-Be elements.

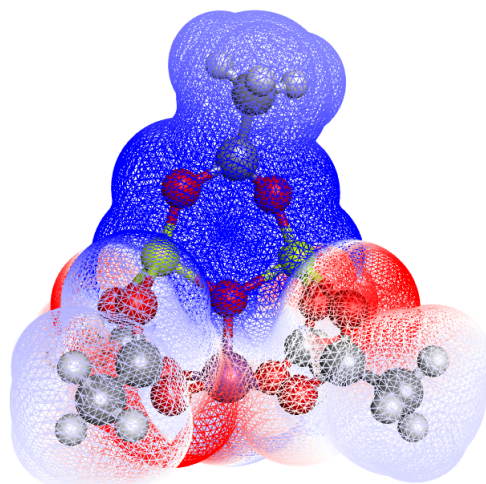


Fig. 17: *Interpolated charge isosurface of BBA*

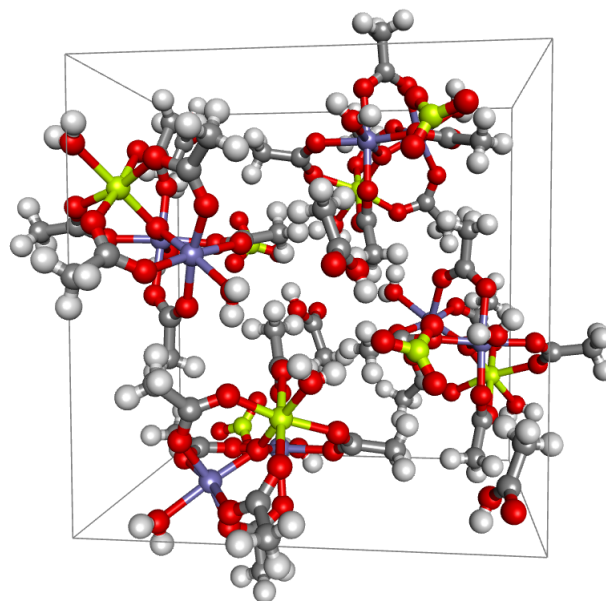


Fig. 18: *RS/EA result of crystal cell prediction*

Predicted radiological properties of BBA

In order to computationally determine the radiation attenuation properties of the BBA salt, the ESTAR database hosted by the National Institute of Standards and Technology (NIST) was used to apply the Bethe collision theory with density-effect correction to the provided molecular formula of BBA, which allowed the attenuation factor for β^- particles to be determined as shown below, as well as the mean ionisation energy which affects the stopping power of the salt with respect to α particles. This was essential to demonstrating that a sufficient α -n conversion rate can be achieved to propagate the cyclic reaction, which requires a reasonably low α stopping power.

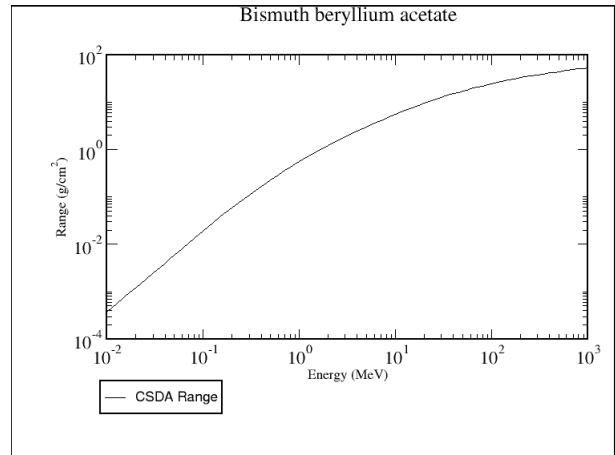


Fig. 21: CSDA range of BBA

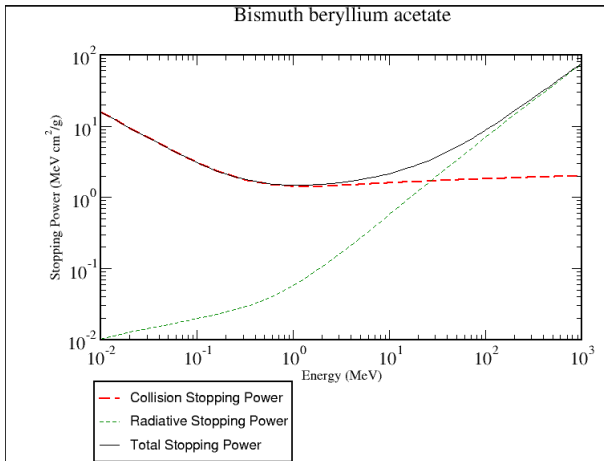


Fig. 19: Stopping power of BBA

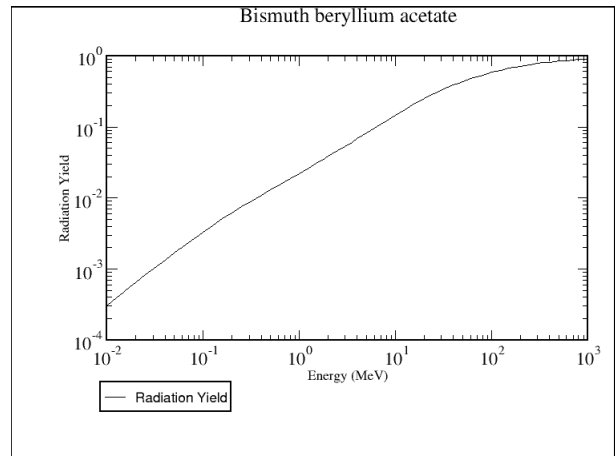


Fig. 22: Radiation yield of BBA

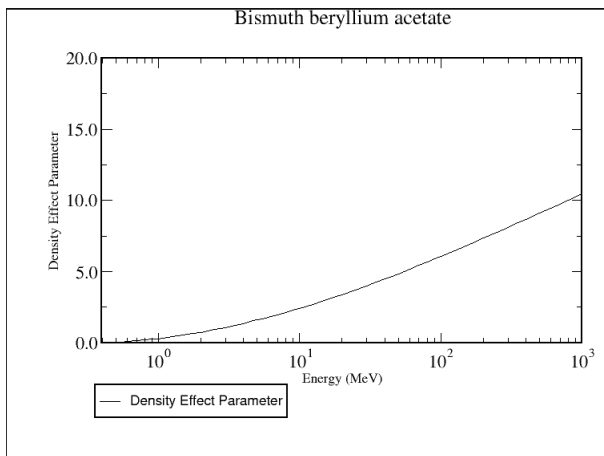


Fig. 20: Density effect parameter of BBA

Appendix B: Neutron source measurements

ARKTIS detector calibration

The calibration curve from the ARKTIS S670e detector is shown below, which was then adapted to obtain the ^{252}Cf neutron spectrum via maxima-corrected retrotransposition.

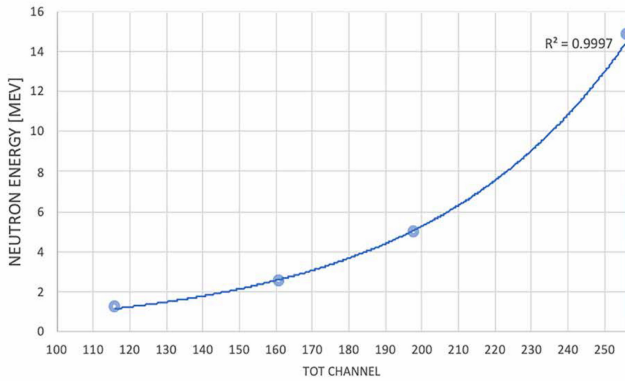


Fig. 23: Literature calibration curve [20]

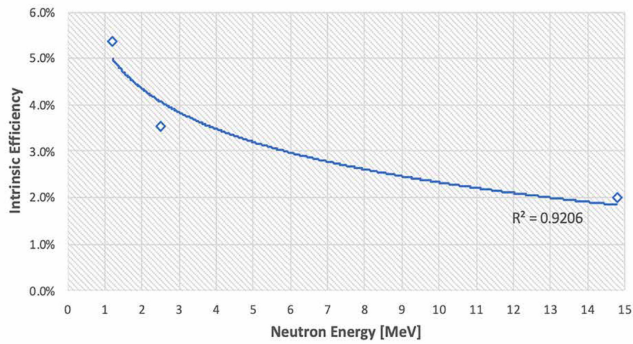


Fig. 24: Intrinsic efficiency curve [20]

Spectrum folding validation

To validate the neutron spectrum, a detector response matrix is first obtained by applying cubic spline interpolation to various detector response curves obtained from literature [20]:

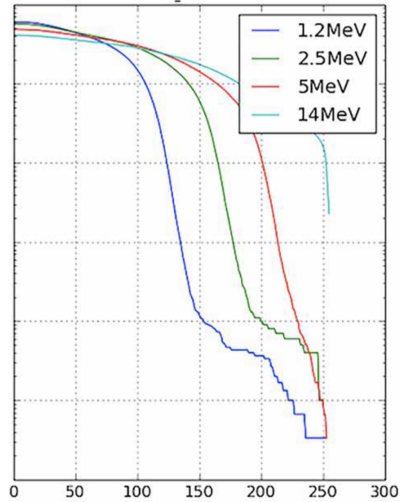


Fig. 25: Detector response curves to various monoenergetic neutron beams [20]

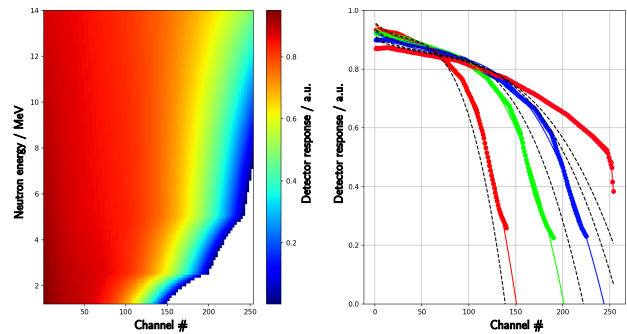


Fig. 26: Detector response matrix

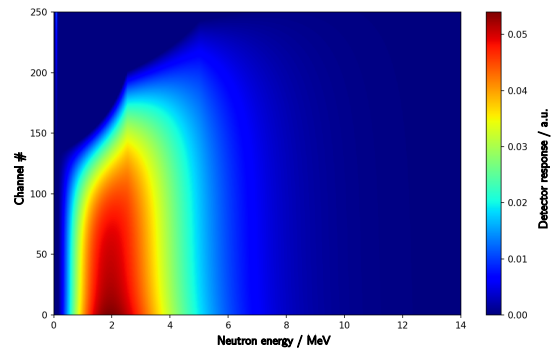


Fig. 27: Folded neutron spectrum

Appendix C: Monte Carlo simulation parameters

To demonstrate the utility of the FOSA assembly in increasing thermal neutron flux within the irradiation cavity, four sets of OpenMC Monte Carlo simulations were run - one set to compare fast neutron flux between the FOSA assembly and a control setup where the ^{252}Cf neutron source is placed behind a moderator with equal thickness as the FOSA apparatus, as well as another set to compare thermal neutron flux between the FOSA and control assembly. The simulation was run on 1000 batches with 10,000 particles each, and transmissive boundary conditions were imposed on the geometric configuration of the irradiation assembly. The ^{252}Cf neutron source was simulated as an isotropic source with a Maxwellian spectrum fitted with our experimental data, and the material of both irradiation assemblies was assumed to be largely polyethylene with a C:H atomic ratio of 1:2. Furthermore, a reasonable assumption was made that thermal Doppler-broadening of neutron scattering cross sections is negligible at the temperature range involved.

To tally the neutron flux over a fixed energy range, the following equation is used to obtain the volume-integrated flux:

$$\phi = \frac{1}{W} \sum_{i \in C} \frac{w_i}{\sigma_t(E_i)} \quad (8)$$

where W is the total neutron mass, w_i is the pre-collision mass of the neutron, and σ_t is the total neutron cross section at energy E_i .

Appendix D: Gamma spectrum analysis

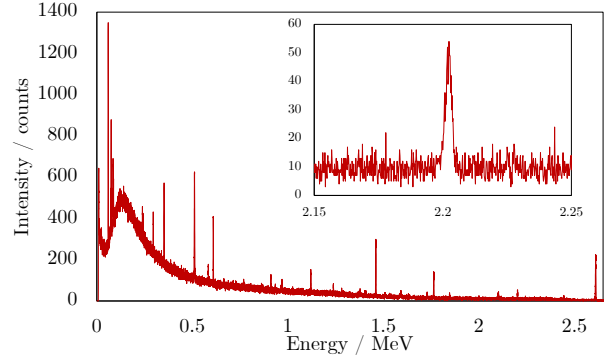


Fig. 28: Gamma-spectrum of irradiated BBA

Table 1. Peak assignment of the irradiated BBA gamma spectrum

Peak energy / keV	Origin
59.54	^{241}Am α decay
238.63	^{212}Pb β^- decay
241.99	^{214}Pb β^- decay
296.00	^{210}Tl β^- decay
351.93	^{214}Pb β^- decay
511.00	positron annihilation
583.19	^{208}Tl β^- decay
609.31	^{214}Bi β^- decay
911.20	^{228}Ac β^- decay
1120.29	^{214}Bi β^- decay
1460.68	^{40}K β^- decay
1764.50	^{214}Bi β^- decay
1847.42	^{214}Bi β^- decay
2200.00	^1H thermal neutron capture
2611.28	^{208}Tl β^- decay